Improving the Safety of Telerobotic Drilling of the Skull Base via Photoacoustic Sensing of the Carotid Arteries

Sungmin Kim, Neeraj Gandhi, Muyinatu A. Lediju Bell, and Peter Kazanzides

***Abstract*— One of the risks of the endonasal approach to skull base surgery is inadvertent damage to one of the two carotid arteries that are located behind the bone being drilled. Photoacoustic imaging, which combines a pulsed laser with an ultrasound receiver probe, has been shown to be able to image blood vessels behind bone. We therefore integrated a photoacoustic imaging system with a telerobotic system, where the pulsed laser is delivered via an optical fiber attached to the drill held by one robot arm and the ultrasound receiver is positioned, at some distance from the drilling site, by another robot arm. This paper describes a new method for accurately determining the safe region for drilling, which is defined by the center-line between the two carotid arteries, and presents the first phantom experiments with this system. The results show that the system can determine the center point with an accuracy better than 2 mm, which suggests that it may be sufficient for clinical scenarios where the two carotid arteries can be within 8 mm of each other.**

I. Introduction

In general, the goal of surgery is to neutralize or resect diseased tissue, while causing minimal damage to surrounding healthy tissue, especially critical anatomy such as major neurovascular structures. In some cases, surgeons can use sight or touch to distinguish between diseased and healthy tissue, but in other cases they must rely on alternative sensing modalities. As a motivating example, we consider the endoscopic transnasal approach to resect pituitary tumors. This approach is minimally invasive and generally effective, but it can result in serious complications such as damage to the carotid artery [1]. While endoscopes or microscopes can provide real-time streaming video of anatomical structures, the visual information is limited to the surface features, which are not always enough to recognize the location of the organs around the surgical area. An endoscope, in particular, cannot detect arteries located behind the bone being drilled. In spite of the availability of a navigation system to visualize surgical instruments with respect to sub-surface anatomy, it is still challenging to provide accurate spatial information of the arteries due to inaccuracies in the registration between the preoperative image and the intraoperative coordinate frame.

Photoacoustic imaging can provide a good solution to overcome the uncertainty about the intraoperative location of the arteries. In contrast with conventional ultrasound imaging, photoacoustic imaging can visualize the target organ in cases where there is an existing obstacle between the ultrasound transducer and target organ, which is the most important characteristic for this study.

This motivates the development of a telerobotic system with photoacoustic image guidance for drilling in transsphenoidal skull base surgery because the photoacoustic image can directly detect the carotid arteries, even when they are located behind the skull bone, and thereby determine the safe drilling region [2]. We consider the safe drilling region to be the area between the two carotid arteries, which are typically separated by a distance of 8-20 mm [3]. The basic concept is to attach an optical fiber to the drill, which shines a pulsed laser into the area being drilled. The pulsed laser has a wavelength that is preferentially absorbed by blood and therefore causes the carotid arteries (if in the path of the laser) to emit acoustic waves that are detected by an externally-mounted ultrasound receiver probe. In prior work, we demonstrated: (1) the feasibility of using photoacoustic imaging to detect anatomical features of interest behind bone [4], [5], (2) a navigation system to guide the alignment of the ultrasound probe and a hand-held instrument containing the laser fiber, which was experimentally shown to localize a simulated carotid artery with respect to the instrument within 1 mm [6], (3) an image-guided telerobotic system similar to the one presented here, but that utilized simulated photoacoustic imaging [6], and (4) experiments with manual and telerobotic sweeping of an optical fiber for measuring critical structures in the photoacoustic image space [7]. The contribution of this paper is to present the system design and phantom experiments of the first telerobotic system that incorporates real-time photoacoustic imaging to determine the safe region for drilling with respect to the robot coordinate system.

II. System Overview

Figure 1 presents an overview of the photoacoustic image-guided telerobotic system, which consists of the Photoacoustic Image Guidance System (PA-IGS) and the research da Vinci Surgical System. The PA-IGS has a photoacoustic imaging module and a photoacoustic image guidance module. The research da Vinci is composed of patient-side robots, a master console, and a workstation. The following sections provide details of these system components; additional information about the system architecture is presented in [8].

A. Photoacoustic Imaging Module

The Photoacoustic Imaging Module (Fig. 2) consists of an Alpinion E-CUBE12R ultrasound system, Alpinion L3-8

S. Kim and P. Kazanzides are with the Department of Computer Science, Johns Hopkins University, Baltimore, MD, USA, and can be contacted at {sungminkim,pkaz}@jhu.edu. M.A.L. Bell is with the Department of Electrical and Computer Engineering and the Department of Biomedical Engineering, Johns Hopkins University. N. Gandhi is with the Department of Electrical and Computer Engineering, University of Virginia, Charlottesville, VA, USA.

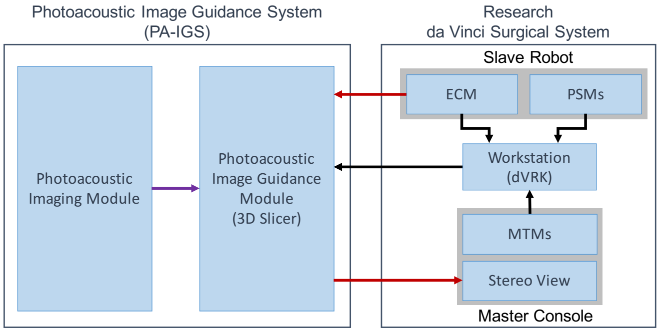

Fig. 1. System architecture for the photoacoustic image-guided telerobotic system; The system consists of the photoacoustic image guidance system and the research da Vinci Surgical System. The black arrows present the flows of the transformation data from the research da Vinci Surgical System, and the red arrows denote the flows of the image data of stereoscope or intraoperative photoacoustic image.

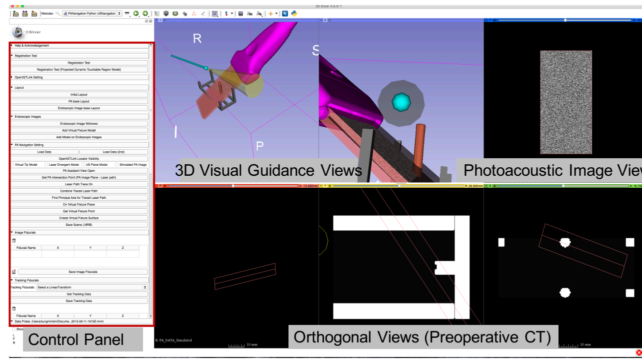

Fig. 3. Photoacoustic Image Guidance module is implemented as a plug-in scripted module for 3D Slicer, which has a control panel (red box on left side) and views for visualization of various information, including the preoperative CT data, intraoperative photoacoustic image data, and 3D visual guidance data.

linear array transducer, and a Laser Components LS Series Pulsed Laser Diode which has 905 nm wavelength coupled to a 1 mm core diameter, 0.5 numerical aperture (NA) multimode optical fiber. In addition, the module has a function generator and power supply to control the laser pulse length and frequency. Photoacoustic images can be generated and displayed in real time on the ultrasound scanner. We developed an image client to receive the images from the ultrasound scanner via a TCP/IP network protocol and transferred these images to the photoacoustic image guidance module of 3D Slicer via OpenIGTLink. The client software is installed on the ultrasound scanner and can provide 8-bit, 16-bit and 32-bit image data.

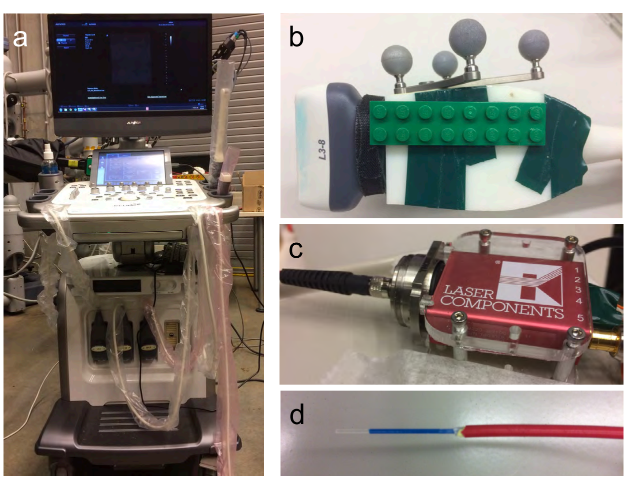

Fig. 2. The photoacoustic imaging system is composed of an (a) Alpinion ECUBE12R ultrasound system, (b) Alpinion L3-8 linear transducer, (c) Laser Components LS Series Pulsed Laser Diode coupled to (d) a multimode optical fiber with a bare cleaved polished tip.

B. *Photoacoustic Image Guidance Module*

The Photoacoustic Image Guidance Module is implemented in Python as a scripted module for 3D Slicer [9] and provides visualization of the spatial relationship between the surgical tools, photoacoustic image, and patient (Figure 3).

The photoacoustic image guidance module has the capability to connect with external tracking systems, robotic systems, and intraoperative imaging systems using the OpenIGTLink network protocol [10]. In this study, the photoacoustic image guidance module is connected to the photoacoustic imaging module and the research da Vinci Surgical System. A tracking system is not required because the da Vinci robot kinematics provide the tracking information that is required to visualize the spatial relationships between the various components in the system. The next section describes the visualization that supports teleoperation by the surgeon, followed by a section that describes the use of photoacoustic imaging as a real-time sensor signal to determine the safe area for drilling by locating and avoiding the carotid arteries.

1) Visualization for Teleoperation: The photoacoustic image guidance module contains models of the surgical tools for visualization of the spatial relationships. Depending on application requirements, the surgical tools can be represented by dimensionally accurate CAD models or by simplified models created using the basic model source of the Visualization Toolkit (VTK) [11]. The photoacoustic image provided by the photoacoustic imaging module can be presented as a 2D plane at the correct location; at the same time, the models of the surgical tools can be placed with respect to their relative positions in the surgical area in the 3D visual guidance views. Furthermore, a virtual laser path is introduced to enable the surgeon to visualize the intersection of the laser path with the surgical area. The virtual laser path is represented by a cone-shaped model that mimics divergence of the real laser beam in tissue.

In addition, the photoacoustic image guidance module provides multiple views for visualizing pertinent information according to the procedures: three orthogonal views for the preoperative CT data, a photoacoustic image view, and two 3D visual guidance views with different viewports. The layout of views can be rearranged according to the application or the surgical procedure.

The photoacoustic image guidance module also provides an additional information window that consists of the photoacoustic image view and a 3D visual guidance view with the surgical tool view, which is displayed on the master console of the telerobotic system as a picture-in-picture view.

The operator can conduct teleoperation while monitoring the spatial relationship of the surgical tools and patient, as well as the photoacoustic image. The photoacoustic image can provide information about critical organs behind the bone surface that cannot be provided by the endoscopic images.

2) Photoacoustic Images as Sensor Signal: Although photoacoustic imaging can detect anatomical features, such as the carotid arteries, even when bony structures block the field of view, it has a fairly narrow field of view due to the narrow divergence of the laser beam. This limitation can be resolved by sweeping the instrument across the sphenoid bone, within the anatomical constraints in endonasal surgery, so that the laser can illuminate different portions of the internal anatomy [6], [7]. Another issue is that the location of the photoacoustic image plane is not accurately known with respect to the robot-held instrument due to errors in the calibration of the ultrasound probe and the kinematics of the robot arms holding the instrument and the ultrasound probe. Thus, while it is possible to locate the carotid arteries in the photoacoustic image (e.g., in a mosaic image created by sweeping the fiber, as in [7]), this location will not be accurately known with respect to the robot instrument. Our proposed solution is to rely on accurate calibration of the laser with respect to the robot instrument, which is possible because they are mechanically integrated. Then, we can consider the photoacoustic image to be a real-time binary sensor signal that indicates whether or not the instrument is in the vicinity of a critical structure.

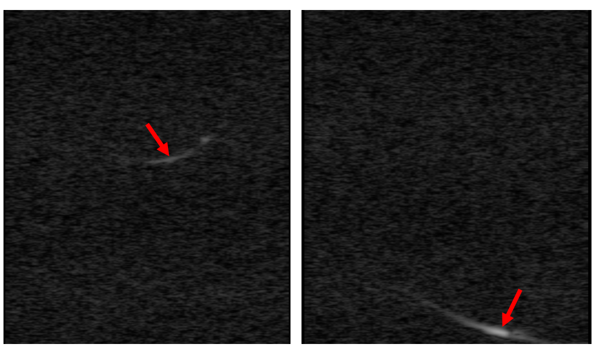

Fig. 4. The photoacoustic images can indicate the existence and location of a target in the region illuminated by the pulsed laser. The edges of the two arteries are shown in these images, which were each created with different laser locations. Note that each image only shows one artery (edge) due to the limited illumination of the laser; the red arrow indicates the detected artery in each photoacoustic image.

Figure 4 shows photoacoustic images of the boundaries of the phantom carotid arteries. While it is possible to observe whether the artery exists in the image, and where it is located in image coordinates, it is not easy to observe its true shape (a cylindrical cross-section). Also, due to the physics of photoacoustic imaging, significantly higher intensity signals are observed on the edges of the artery. Thus, we adopt a method that extracts a minimal amount of information from each photoacoustic image. Specifically, as the fiber is swept, the system extracts the maximum intensity from each photoacoustic image (Fig. 5). As will be demonstrated in the experiments, this is sufficient to detect the edges of both carotid arteries (if the sweep is wide enough) or to detect the valley (safe region) between the peaks corresponding to the carotid arteries (for a more limited sweep).

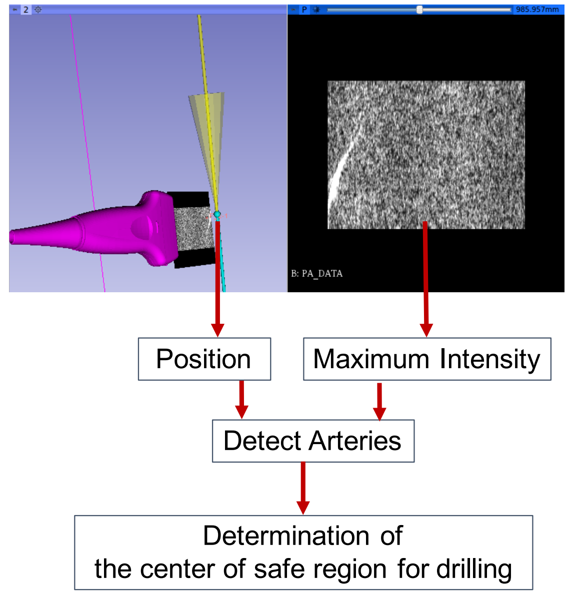

Fig. 5. The edges of the artery can be detected by considering significantly high intensity of the photoacoustic image during sweeping of the optical fiber; the edge positions can be used to determine the center of the safe region for drilling.

C. Telerobotic System: Research da Vinci Surgical System

The telerobotic system is developed based on the first generation da Vinci Surgical System, which can provide three Patient Side Manipulators (PSMs) and one Endoscopic Camera Manipulator (ECM) on the patient side (Fig. 6-left), and two Master Tool Manipulators (MTMs) for teleoperation on the master side (Fig. 6-right). The teleoperation and data flow in the telerobotic system are controlled by the da Vinci Research Kit (dVRK) electronics and software [12].

Each PSM and ECM of the research da Vinci Surgical system consists of a passive setup joint and an active arm. The setup joint is passively manipulated to determine the position and orientation of the active arm for teleoperation. This system included a prototype interface between the da Vinci Research Kit electronics and the passive setup joints to obtain the position and orientation of each setup joint. Using the position and orientation of the setup joints and active arms, the tool position and orientation was obtained, which provided tool tracking using only the kinematic information of the research da Vinci Surgical System.

We recognize that our first-generation da Vinci system is not ideally designed for endonasal skull base surgery. In particular, the endoscope diameter is too large, there is no existing drill instrument, and the PSMs (and instruments themselves) have more compliance than would be desirable for a drilling operation. Nevertheless, it provides a convenient platform for prototype evaluations with phantoms.

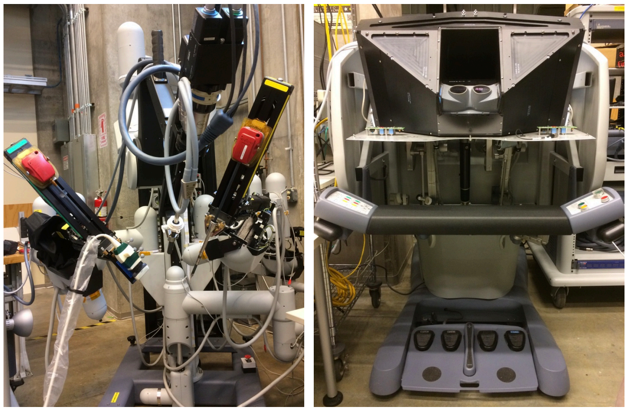

Fig. 6. The da Vinci Surgical System provides multiple arms on the patient side (left), and teleoperation via the master tool manipulators (right).

III. Experiments

A. Phantom

The phantom (Fig. 7) was designed using 3D CAD software (SolidWorks, Dassault Systems) and built by assembling acrylic parts cut by a laser cutting machine. It is composed of an inner box and an outer box. Two rubber rods are attached on the inner box to represent the carotid arteries. The position of the arteries can be adjusted by changing the position of the artery holder; the height of the inner box also can be adjusted by changing the size of the wood block between the inner and outer boxes. For these experiments, we did not include bone (or similar hard material) because our experimental setup did not provide adequate protection to allow us to safely use a laser with sufficient power to create photoacoustic images through bone. Nevertheless, we previously demonstrated that this is possible with real bone [4].

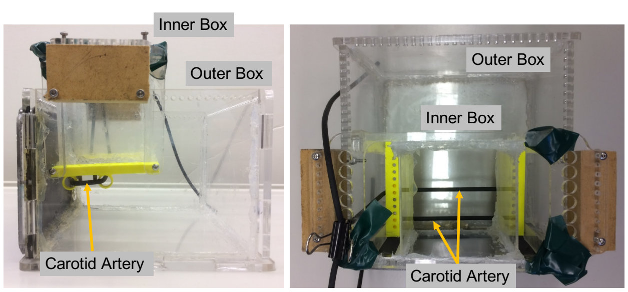

Fig. 7. The phantom consists of an inner box and an outer box; the rubber rods (arteries) are attached to the inner box. Left is front view image, and right is top view image.

B. Experimental Setup

Figure 8 presents the experimental setup for this phantom study. One MTM, two PSMs, and the ECM of the research da Vinci Surgical System were used for this study (Fig. 8-left). PSM1 has an optical fiber attached to a standard da Vinci instrument to mimic the endoscopic surgical drill. Although a single optical fiber was used in these experiments, multiple optical fibers could be employed for specialized light delivery around the surgical tool [13]. PSM2 supports the ultrasound transducer via a custom attachment to the trocar mount. The photoacoustic image guidance system provides visualization of the spatial relationship between the ultrasound transducer, photoacoustic image, surgical tool (drill), and virtual laser beam using kinematics-based tracking data. Furthermore, the PA-IGS system provides visual guidance for teleoperation through the additional information view on the stereo view of the master console. In addition, the real-time photoacoustic image can be presented in the additional information view and in the main window of 3D Slicer, respectively (Fig. 8-right).

The phantom filled with water was placed on the table near the research da Vinci Surgical System and the ECM was set up to provide stereo visualization of the experimental procedure. The ultrasound transducer on PSM2 was placed on the side of the phantom to receive the photoacoustic signals and the surgical tool with optical fiber (PSM1) was placed near the experimental area (Fig. 8-middle).

C. Photoacoustic Imaging

Real photoacoustic images were acquired from the photoacoustic imaging system. The dimension of each photoacoustic image is 568 x 596, with 16-bit pixels of size 0.0669 mm x 0.0755 mm. The data was transferred from the photoacoustic imaging system to the PA-IGS via OpenIGTLink.

D. Experimental Procedure

The surgical tool with the optical fiber was swept from the left artery to the right artery on the phantom by teleoperation. During this operation, the position and orientation of the surgical tool was collected, along with the photoacoustic measurement (highest intensity value), as described in Section II-B.2. After the sweeping motion, each artery edge was detected by thresholding the photoacoustic sensing data. The measurements for the diameter of the arteries and the distance between the arteries are calculated based on the detected edge data. Finally, the safe region is defined as the area between the two arteries, and the center of the safe region for skull base drilling is determined.

IV. Results

Figure 9 shows the photoacoustic measurements from 5 trials, obtained by recording the maximum intensity in each photoacoustic image as the laser is swept across the phantom. Each plot has 4 peaks that correspond to the edges of the two arteries. Based on the detected edges, the size of each artery and the distance between the arteries were measured, as presented in Table I. According to the distance measured using photoacoustic imaging, the diameters of the left artery and right artery are 3.40 mm and 3.49 mm, respectively, which are similar to the ground-truth measurement of 3.26 mm obtained using calipers. The distance between the two arteries is 19.68 mm, which is also close to the caliper measurement of 19.50 mm. The standard deviations for the measurements are 0.59 mm and 0.62 mm for the artery diameters and 0.39 mm for the distance between the arteries.

The photoacoustic measurements in Fig. 9 were obtained by collecting the positions of the surgical tool, thereby allowing all collected data to be presented in 3D space. In particular,

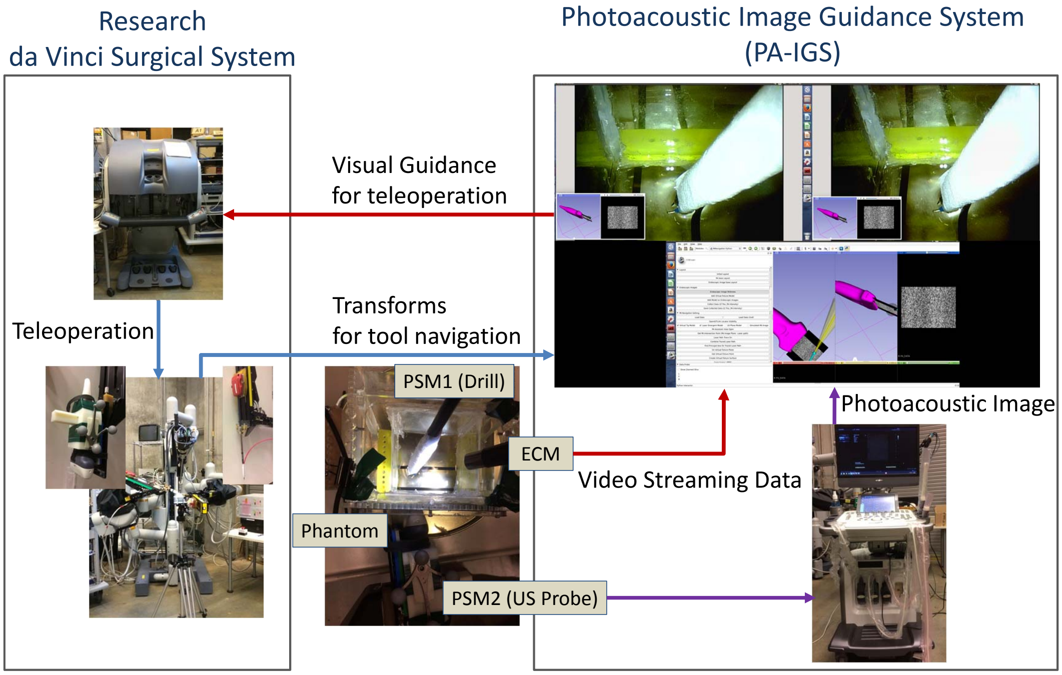

Fig. 8. Experimental setup, showing research da Vinci System (left), closeup view of phantom (middle), visualization provided by Photoacoustic Image Guidance System (top right) and photoacoustic imaging system (bottom right).

based on the locations of the edges, we can identify the safe region and determine its center, as tabulated in Table II. As shown in the table, the estimation of the center of the safe region shows good repeatability between the five trials, with standard deviations less than 1 mm for each coordinate.

To provide a ground-truth measurement, we teleoperated the da Vinci surgical tool to touch two points on the inner surfaces of each artery, which allowed us to define a line corresponding to the inner surface of each artery. Table III shows the distance from each determined center point to the lines corresponding to the left and right arteries. On average, the determined center point is within 1.1 mm of the ground-truth center point. We note, however, that the ground truth measurement is not extremely accurate because it relies on the kinematics of the da Vinci robot.

TABLE I

DIAMETERS AND DISTANCES BASED ON PHOTOACOUSTIC MEASUREMENT

	Diameter, mm (Left Artery)	Distance, mm (between Arteries)	Diameter, mm (Right Artery)
Trial 1	3.61	19.99	2.77
Trial 2	3.97	19.02	4.38
Trial 3	2.80	19.79	3.56
Trial 4	3.87	19.67	3.07
Trial 5	2.74	19.96	3.64
Mean	3.40	19.68	3.49
S.D.	0.59	0.39	0.62

TABLE II

COORDINATES OF THE DETERMINED CENTER OF THE SAFE REGION

	X, mm	Y, mm	Z, mm
Trial 1	-232.79	1234.84	1757.91
Trial 2	-234.63	1236.81	1757.91
Trial 3	-234.26	1235.38	1758.25
Trial 4	-234.43	1234.76	1758.29
Trial 5	-233.98	1234.53	1758.52
Mean	-234.02	1235.26	1758.17
S.D.	0.73	0.92	0.27

TABLE III

ACCURACY OF DETERMINING THE CENTER OF THE SAFE REGION

	Distance to Left Artery, mm	Distance to Right Artery, mm	Off-Center mm
Trial 1	10.78	11.32	0.27
Trial 2	10.28	12.01	0.86
Trial 3	9.95	12.44	1.24
Trial 4	9.52	12.85	1.67
Trial 5	9.83	12.66	1.42
Mean	10.07	12.56	1.09
S.D.	0.48	0.61	0.54

V. DISCUSSION AND CONCLUSIONS

We previously developed a photoacoustic image guidance system [14], and a telerobotic system based on the research da Vinci Surgical System and synthetic photoacoustic images [6]. At the same time, we explored the feasibility of photoacoustic imaging for skull base surgery in benchtop setups [4], [15]. These previous works (and [7]) primarily considered photoacoustic imaging as an intraoperative imaging modality. In this study, however, we propose use of the photoacoustic image as a real-time sensor signal. The photoacoustic measurement can provide information about whether or not the target (critical structure) is in the path of the laser beam. By combining this signal with the position of the surgical tool, we can better estimate the target position. More specifically, to reduce the risk of damage to the carotid arteries we can use the

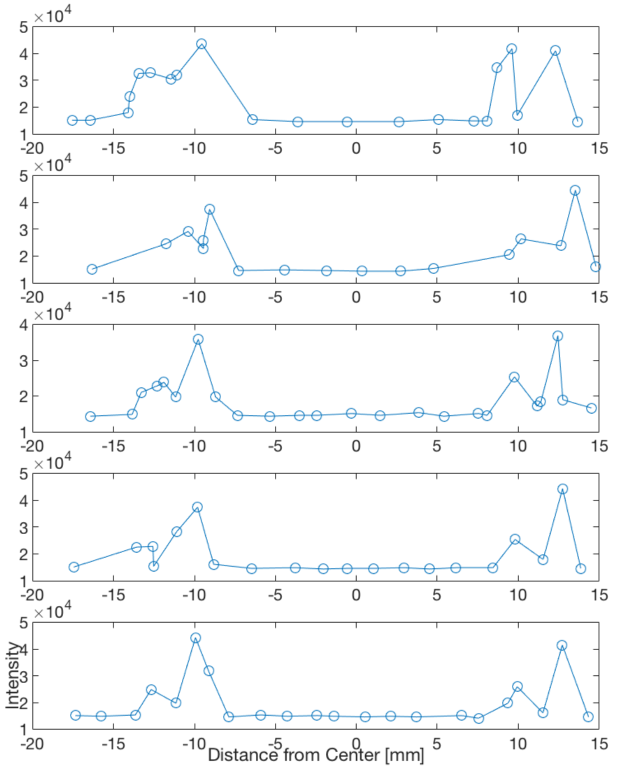

Fig. 9. The photoacoustic measurements during a sweeping motion of the surgical tool. Each plot is the result of one trial, corresponding (from top to bottom) to trials 1-5. Intensities are represented in image pixel values.

photoacoustic measurement to determine the center point of the safe area between the carotid arteries, even when they are located behind bone. This center point can provide the recommended drilling area that affords the greatest clearance with respect to the carotid arteries. Furthermore, by extracting just the maximum intensity of the photoacoustic image, we lessen the effect of latency between measurement of the surgical tool position and acquisition of the photoacoustic image, as well as the effect of any errors in the calibration of the ultrasound probe with respect to the robot. In the worst case, an uncalibrated ultrasound transducer could be used, as long as it can be placed at a proper location to observe the photoacoustic images. This could, for example, be achieved by having the robot sweep the uncalibrated US probe until a photoacoustic signal is detected.

We demonstrate the determination of the safe region for skull base surgery using photoacoustic measurement on a telerobotic system. Our system shows promising results by accurately measuring the diameters of the two simulated arteries as well as the distance between them. More importantly, determination of the center of the safe region is shown to be repeatable over five trials and within 2 mm of the estimated true center. These results suggest that photoacoustic imaging, when combined with robotic positioning, can create a map of the arteries behind the bone. Note, however, that photoacoustic imaging requires sufficient laser energy to penetrate the bone. Thus, it is unlikely to produce an image prior to the start of drilling, and will therefore require the surgeon to begin drilling until the bone thickness is sufficiently reduced to enable photoacoustic imaging.

Although studied in the context of endonasal skull base surgery, this system could be used in other applications; for example, to locate arteries or veins for needle injections into obese patients. Future work includes testing of this system in more realistic environments, using anatomical phantoms or cadavers.

VI. Acknowledgments

This work was supported by NSF NRI 1208540 (PI: P. Kazanzides) and NIH K99-EB018994 awarded to M.A. Lediju Bell. N. Gandhi received support from the NSF REU program via EEC-1460674. Youri Tan and Anton Deguet assisted with software development for the research da Vinci robot.

References

[1] P. Cappabianca, L. M. Cavallo, A. Colao, and E. de Divitiis, "Surgical complications associated with the endoscopic endonasal transsphenoidal approach for pituitary adenomas," *Journal of Neurosurgery*, vol. 97, no. 2, pp. 293–298, Aug 2002.

[2] M. A. L. Bell, A. K. Ostrowski, K. Li, P. Kazanzides, and E. M. Boctor, "Localization of transcranial targets for photoacoustic-guided endonasal surgeries," *Photoacoustics*, vol. 3, no. 2, pp. 78–87, 2015.

[3] W. H. Renn and A. L. Rhoton Jr, "Microsurgical anatomy of the sellar region," *Journal of Neurosurgery*, vol. 43, no. 3, pp. 288–298, 1975.

[4] M. A. Lediju Bell, A. K. Ostrowski, P. Kazanzides, and E. Boctor, "Feasibility of transcranial photoacoustic imaging for interventional guidance of endonasal surgeries," in *SPIE Photonics West*, vol. 8943, Feb 2014.

[5] M. A. L. Bell, A. B. Dagle, P. Kazanzides, and E. M. Boctor, "Experimental assessment of energy requirements and tool tip visibility for photoacoustic-guided endonasal surgery," in *SPIE BiOS*. International Society for Optics and Photonics, 2016, pp. 97 080D–97 080D.

[6] S. Kim, Y. Tan, P. Kazanzides, and M. A. Lediju Bell, "Feasibility of photoacoustic image guidance for telerobotic endonasal transsphenoidal surgery," in *IEEE Intl. Conf. on Biomedical Robotics and Biomechatronics (BioRob)*, June 2016, pp. 482–488.

[7] N. Gandhi, S. Kim, P. Kazanzides, and M. A. L. Bell, "Accuracy of a novel photoacoustic-based approach to surgical guidance performed with and without a da Vinci robot," in *SPIE Photonics West*, San Francisco, CA, Jan 2017.

[8] S. Kim, Y. Tan, A. Deguet, and P. Kazanzides, "Real-time image-guided telerobotic system integrating 3D Slicer and the da Vinci Research Kit," in *The First IEEE Intl. Conf. on Robotic Computing*, Taichung, Taiwan, April 2017.

[9] S. D. Pieper, M. Halle, and R. Kikinis, "3D Slicer," in *IEEE Intl. Symp. on Biomedical Imaging (ISBI)*, Apr 2004, pp. 632–635.

[10] J. Tokuda, G. S. Fischer, X. Papademetris, Z. Yaniv, L. Ibanez, P. Cheng, H. Liu, J. Blevins, J. Arata, A. J. Golby, T. Kapur, S. Pieper, E. C. Burdette, G. Fichtinger, C. M. Tempany, and N. Hata, "OpenIGTLink: an open network protocol for image-guided therapy environment," *Intl. J. of Medical Robotics and Computer Assisted Surgery*, vol. 5, no. 4, pp. 423–434, 2009.

[11] W. J. Schroeder, K. M. Martin, and W. E. Lorensen, *The Visualization Toolkit*, 4th ed. Kitware, Dec. 2006.

[12] P. Kazanzides, Z. Chen, A. Deguet, G. S. Fischer, R. H. Taylor, and S. P. DiMaio, "An open-source research kit for the da Vinci® surgical system," in *IEEE Intl. Conf. on Robotics and Automation (ICRA)*, Hong Kong, China, June 2014.

[13] B. Eddins and M. A. L. Bell, "Design of a multifiber light delivery system for photoacoustic-guided surgery," *J. Biomedical Optics*, vol. 22, no. 4, 2017.

[14] S. Kim, H. J. Kang, A. Cheng, M. A. Lediju Bell, E. Boctor, and P. Kazanzides, "Photoacoustic image guidance for robot-assisted skull base surgery," in *IEEE Intl. Conf. on Robotics and Automation (ICRA)*, May 2015, pp. 592–597.

[15] M. A. Lediju Bell, A. K. Ostrowski, K. Li, P. Kazanzides, and E. Boctor, "Quantifying bone thickness, light transmission, and contrast interrelationships in transcranial photoacoustic imaging," in *SPIE Photonics West*, Feb 2015.